Electronic Supplementary Material (ESI) for Journal of Materials Chemistry C.

SUPPORTING INFORMATION

Novel gold(I) diphosphine-based dimers with aurophilicity-triggered multistimuli light-emitting properties

Csaba Jobbágy,[a] Péter Baranyai,[a] Gábor Marsi,[a] Barbara Rácz,[a] Liang Li,[b]
Pance Naumov*[b] and Andrea Deák*[a]

[a] Hungarian Academy of Sciences, MTA TTK SZKI,
"Lendület" Supramolecular Chemistry Research Group,
1117 Budapest, Magyar Tudósok körútja 2, Hungary;
E-mail: deak.andrea@ttk.mta.hu

[b] New York University Abu Dhabi, P.O. Box 129188,
Abu Dhabi, United Arab Emirates;
E-mail: pance.naumov@nyu.edu

Compound **1**: Yield: 0.423g (88%); HRMS–ESI (*m/z*): $\{[Au_2(dpephos)_2]NO_3\}^+$ calcd for $C_{72}H_{56}NO_5P_4Au_2$, 1532.244; found, 1532.237.

Fig. S1 HRMS-ESI spectra of **1**.

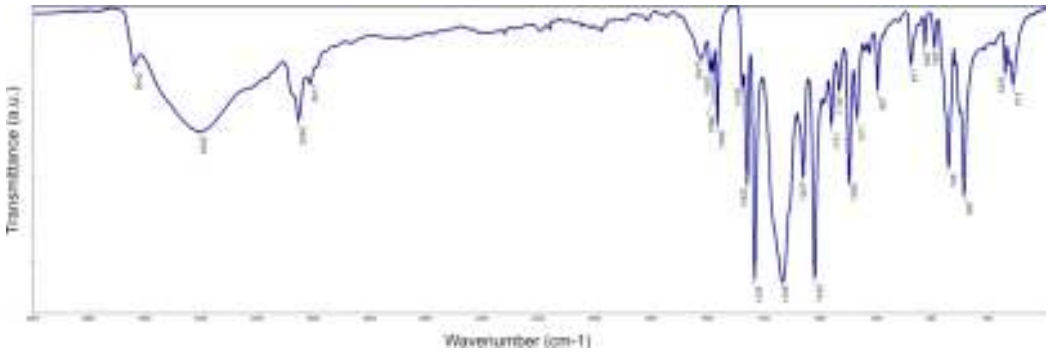

Fig. S2 FTIR spectra of compound **1**.

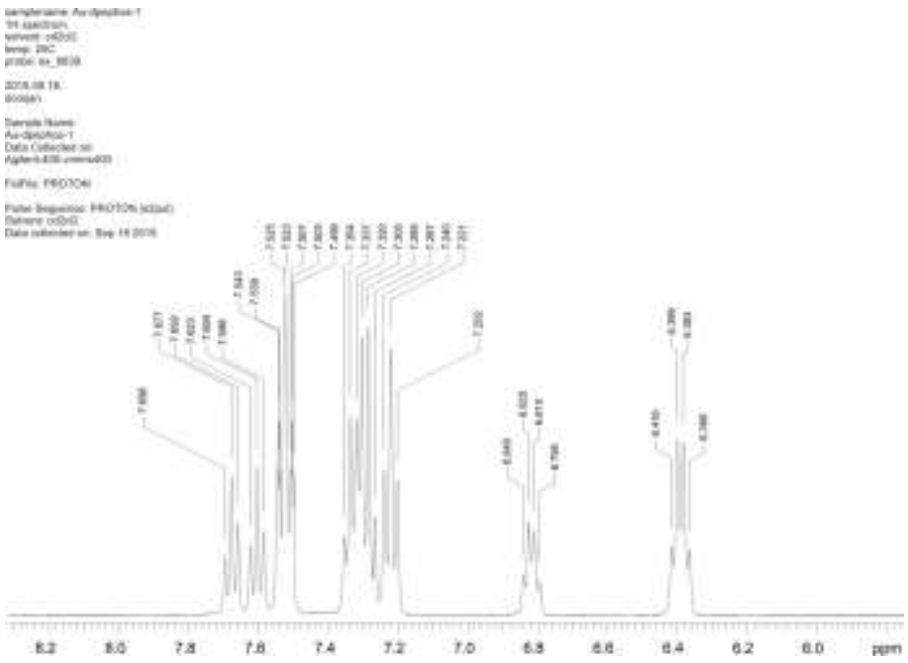

Fig. S3 ^{1}H-NMR spectra of compound **1**.

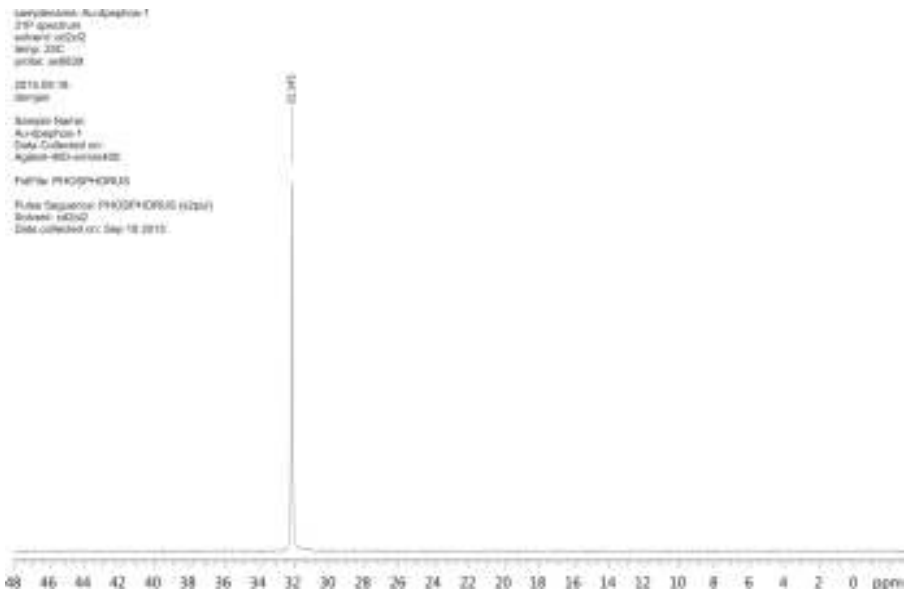

Fig. S4 ^{31}P-NMR spectra of compound **1**.

Compound **2**: Yield: 0.354g (85%); HRMS–ESI (*m/z*): $\{[Au_2(dpephos)_2]CF_3SO_3\}^+$ calcd for $C_{73}H_{56}O_5F_3P_4SAu_2$, 1619.208; found, 1619.196.

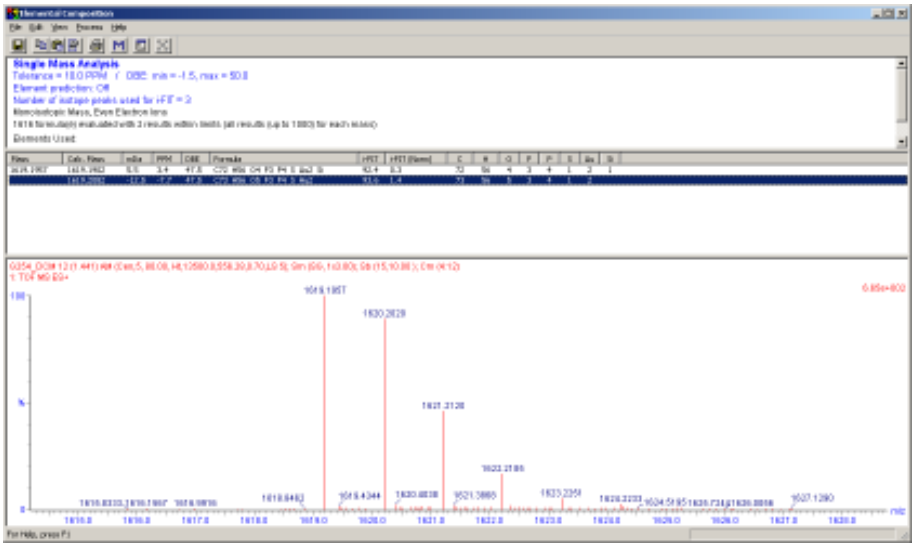

Fig. S5 HRMS-ESI spectra of **2**.

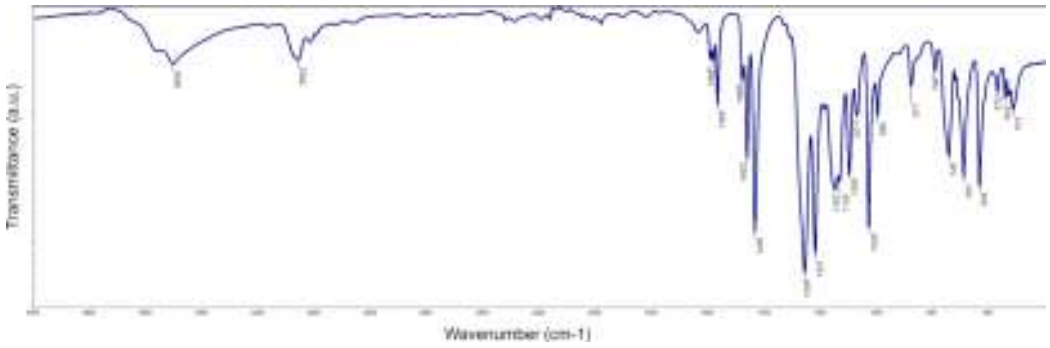

Fig. S6 FTIR spectra of compound **2**.

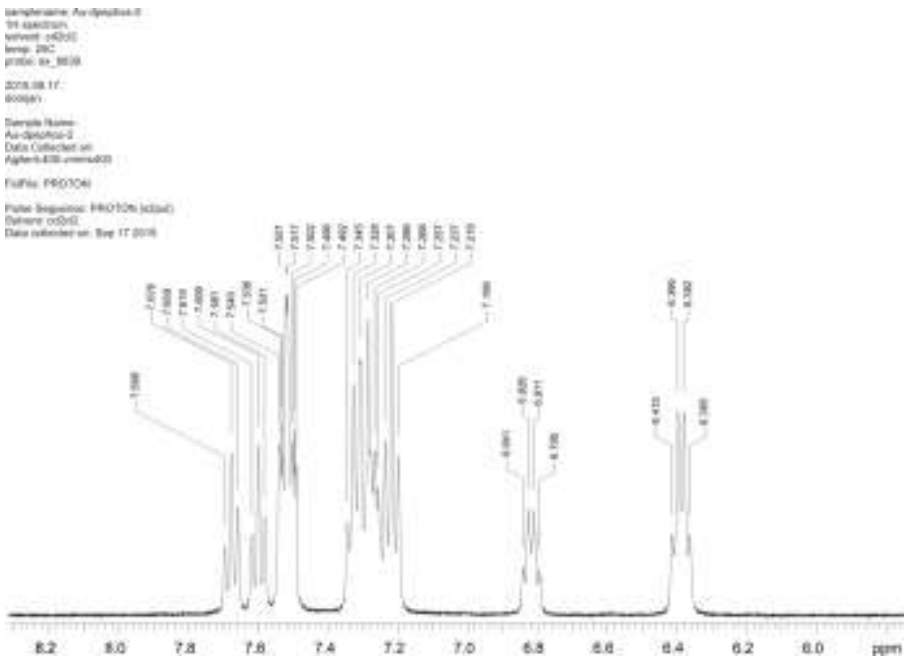

Fig. S7 ^{1}H-NMR spectra of compound **2**.

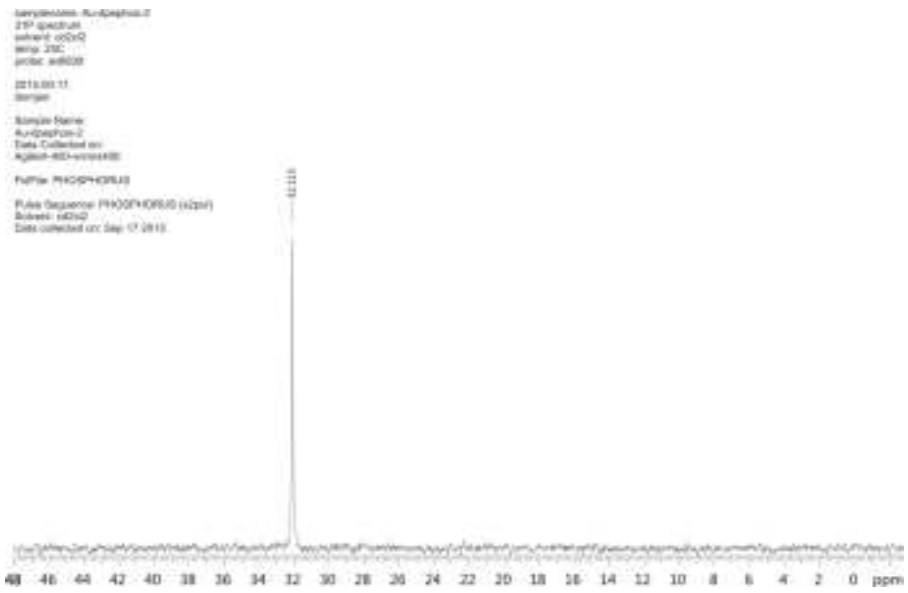

Fig. S8 ^{31}P-NMR spectra of compound **2**.

Compound **3**: Yield: 0.175g (79%); HRMS–ESI (*m/z*): $\{[Au_2(dpephos)_2]BF_4\}^+$ calcd for $C_{72}H_{56}{}^{10}BO_2F_4P_4Au_2$, 1556.263; found, 1556.270.

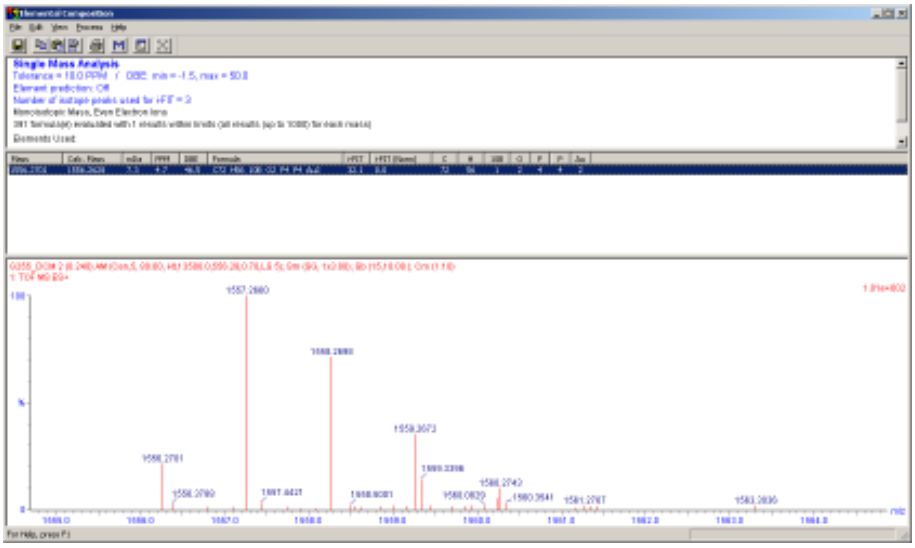

Fig. S9 HRMS-ESI spectra of **3**.

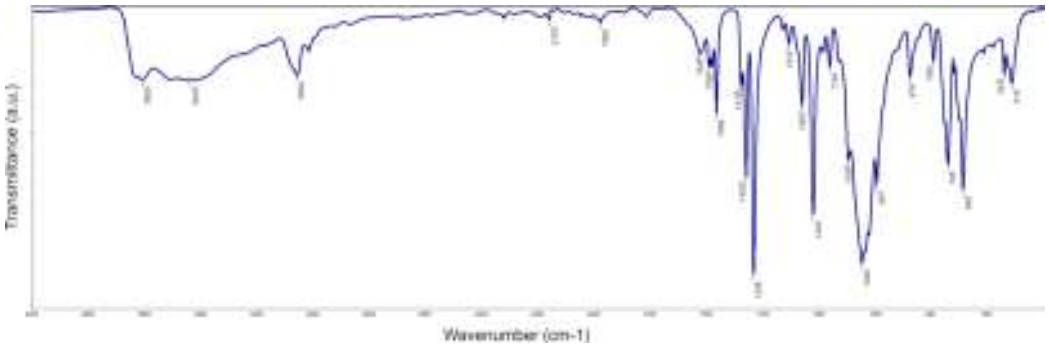

Fig. S10 FTIR spectra of compound **3**.

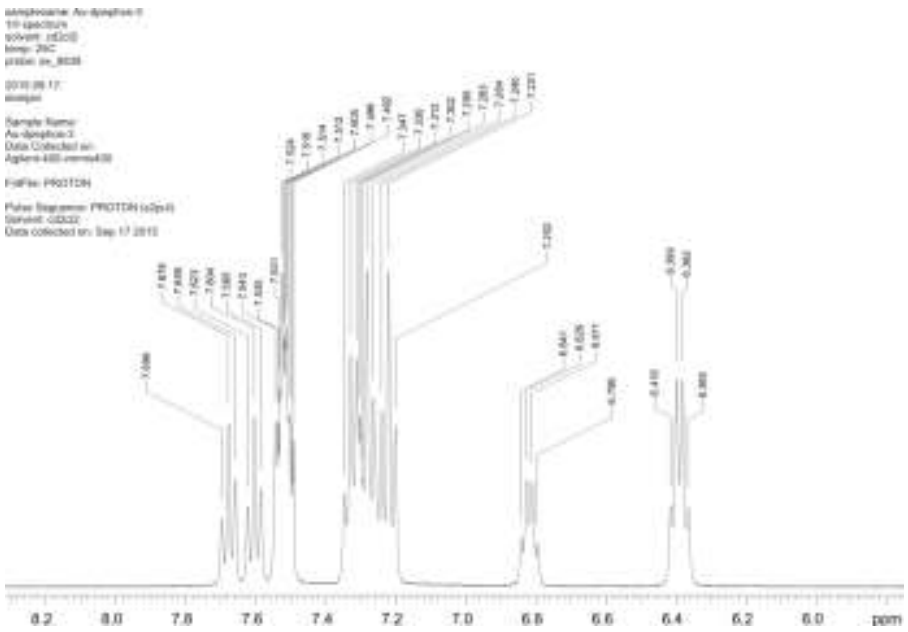

Fig. S11 ^{1}H-NMR spectra of compound **3**.

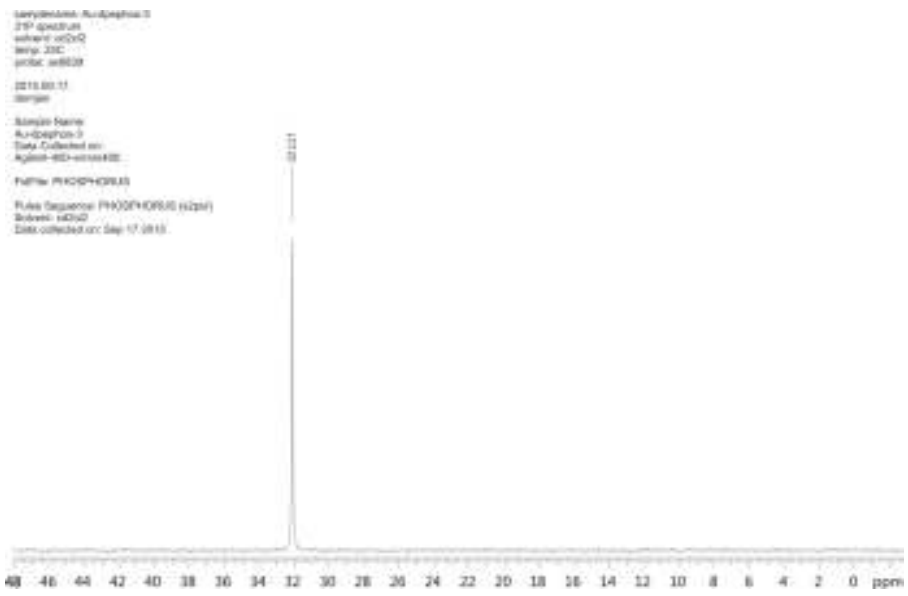

Fig. S12 ^{31}P-NMR spectra of compound **3**.

Compound **4**: Yield: 0.322g (92%); HRMS–ESI (*m/z*): $\{[Au_2(dpephos)_2]PF_6\}^+$ calcd for $C_{72}H_{56}O_2F_6P_5Au_2$, 1615.220; found, 1615.216.

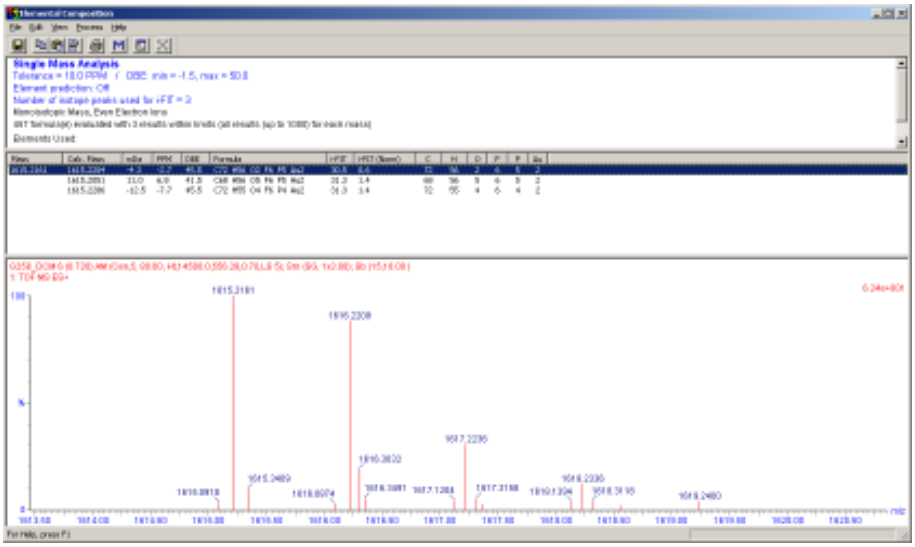

Fig. S13 HRMS-ESI spectra of **4**.

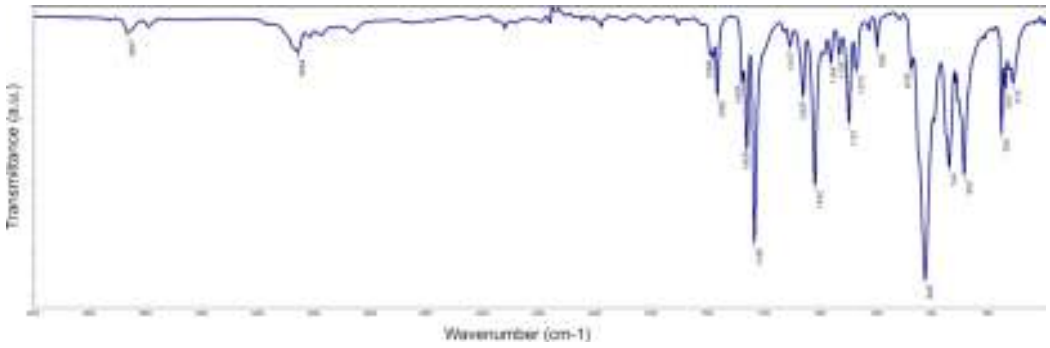

Fig. S14 FTIR spectra of compound **4**.

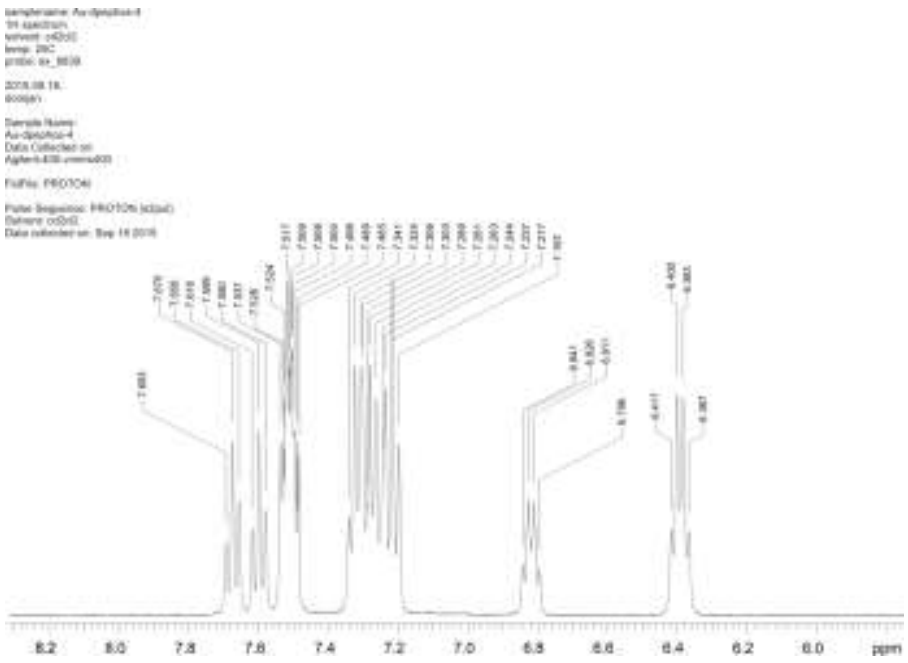

Fig. S15 ^{1}H-NMR spectra of compound **4**.

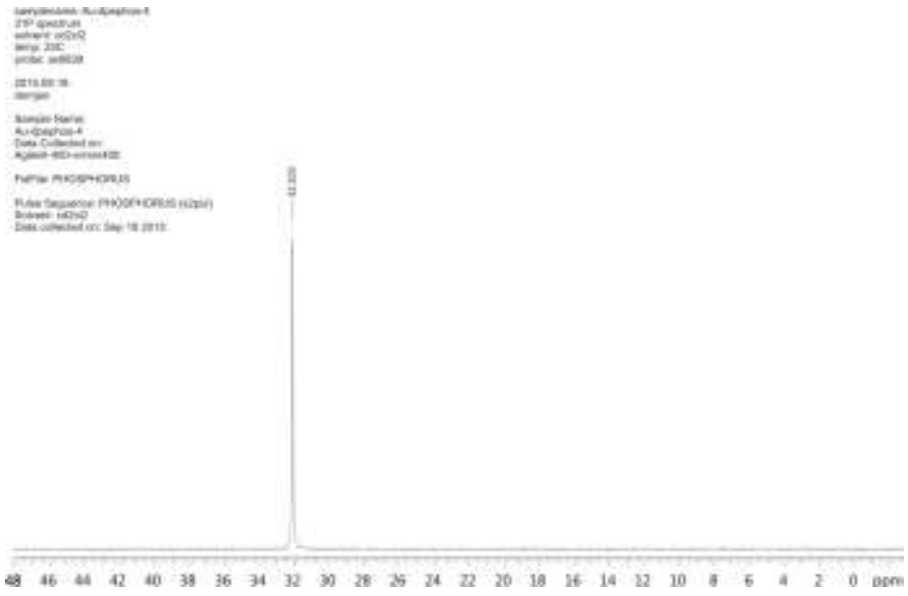

Fig. S16 ^{31}P-NMR spectra of compound **4**.

Compound **5**: Yield: 0.358g (92%); HRMS–ESI (*m/z*): $\{[Au_2(dpephos)_2]SbF_6\}^+$ calcd for $C_{72}H_{56}O_2F_6P_4SbAu_2$, 1705.150; found, 1705.152.

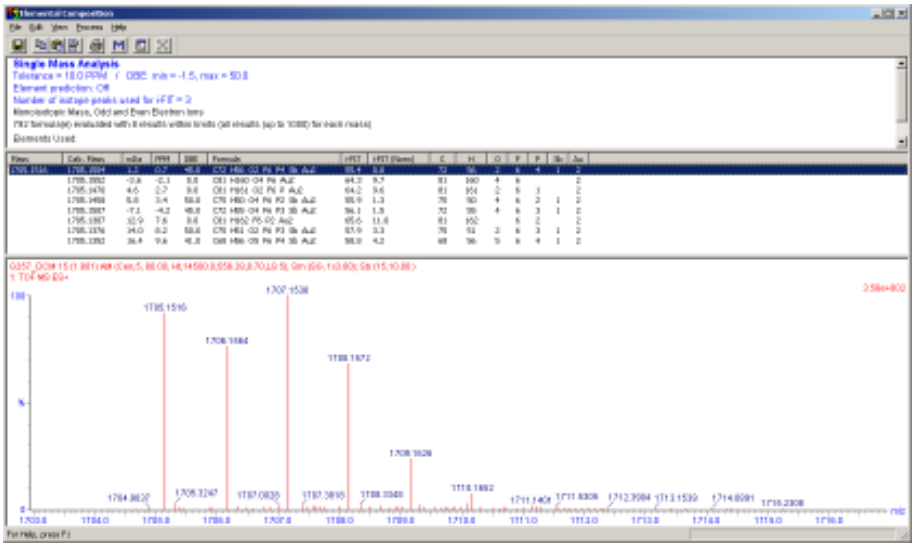

Fig. S17 HRMS-ESI spectra of **5**.

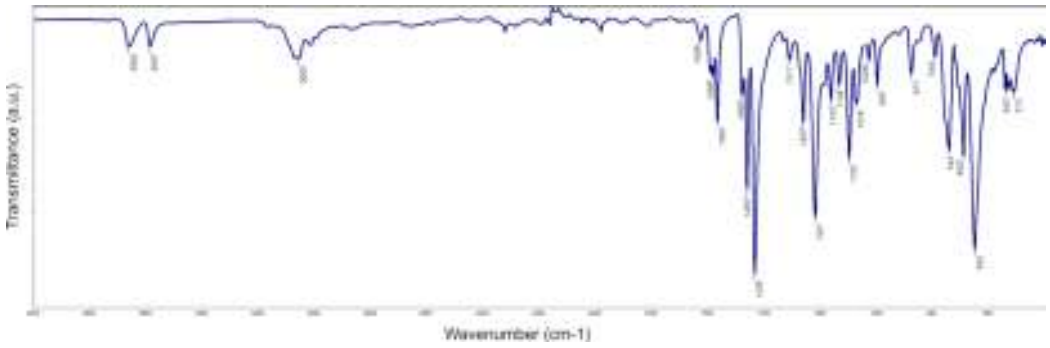

Fig. S18 FTIR spectra of compound **5**.

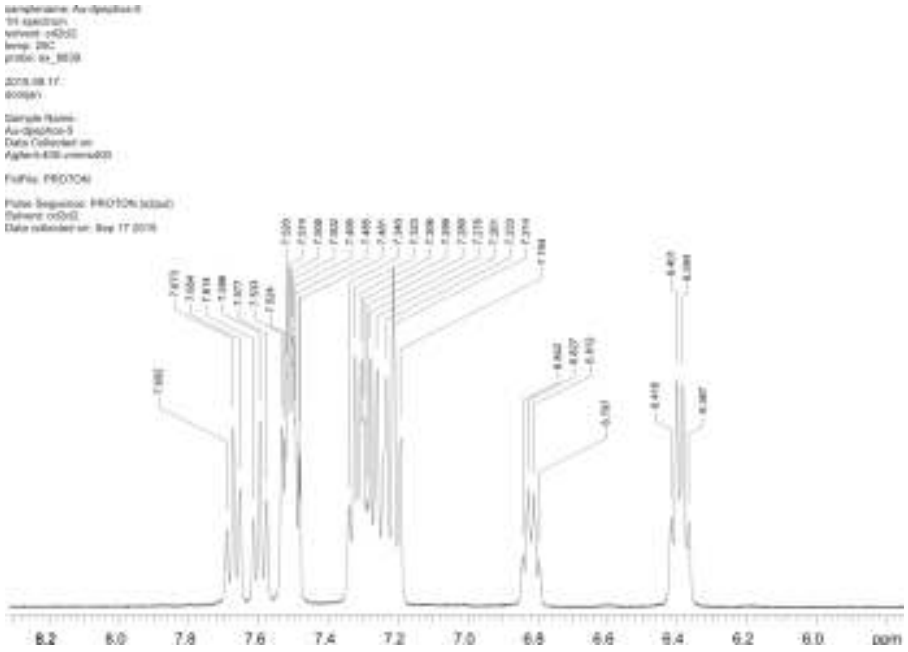

Fig. S19 ^{1}H-NMR spectra of compound **5**.

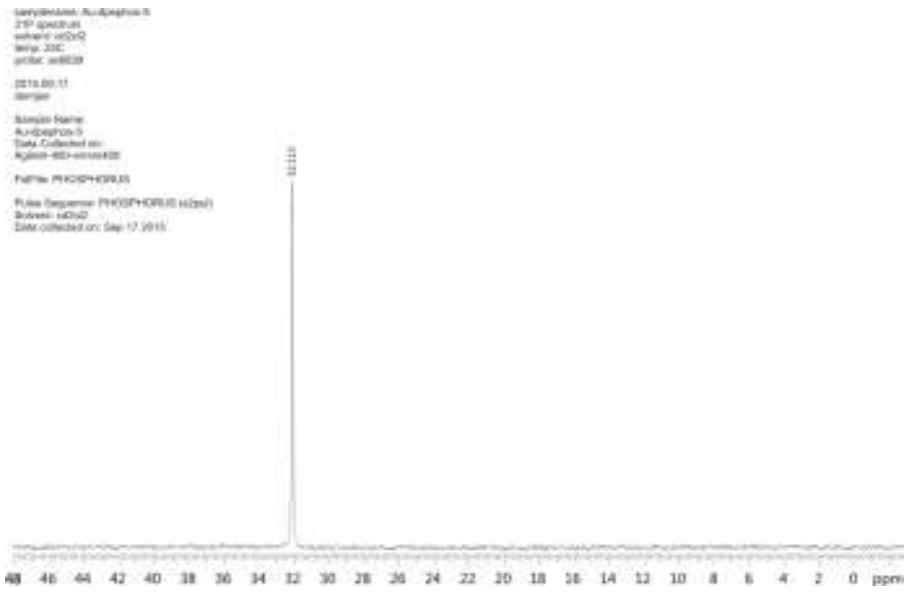

Fig. S20 ^{31}P-NMR spectra of compound **5**.

Fig. S21 Twist-boat conformation of $[Au_2(dpephos)_2]^{2+}$ skeleton with Au···Au axis perpendicular to the page. Colour scheme: gold, yellow; phosphorous, orange; carbon, grey; oxygen, red;. Hydrogen atoms and phenyl groups have been omitted.

Computational studies

In the present study density functional theory (DFT) and time-dependent density functional theory (TD DFT) calculations were performed by using the *Gaussian 09* program package[1] at the M06/6-31G* level of theory.[2] Relativistic effects were included for the Au atom by using the Los Alamos National Laboratory double zeta type (LANL2DZ) pseudopotential. The geometries of the singlet ground state (S_0) and triplet excited state (T_1) of the $[Au_2(dpephos)_2]^{2+}$ cation were fully optimized in the gas phase without symmetry constraints. Due to convergence problems with the TD DFT optimization, the structure for the lowest triplet excited states (T_1) of the complex cation was optimized with the unrestricted UM06/LAN2LDZ method. After geometry optimization the excited states were investigated by TD DFT analysis. The absorption energies were obtained by TD DFT method at the optimized ground state geometry using the same functional and basis sets as for geometry optimization. The lowest energy triplet emission was determined by TD DFT calculation with M06 functional at the optimized triplet (T_1) structure. The molecular orbital surfaces were plotted by Molekel 5.4 visualization software at an isosurface value of 0.03 au.[3]

Table S1 Selected bond lengths (Å), bond angles (°) and torsion angles (°) in optimized singlet ground state (S_0) and triplet excited state (T_1) structures of $[Au_2(dpephos)_2]^{2+}$ cation.

	S_0	**T_1**
Au(1)−P(1)	2.389	2.487
Au(1)−P(3)	2.391	2.489
Au(2)−P(2)	2.362	2.381
Au(2)−P(4)	2.365	2.382
Au(1)···Au(2)	3.371	2.942
P(1)–Au(1)−P(3)	161.53	112.46
P(2)–Au(2)−P(4)	175.85	175.76
P(1)–C(1)–C(8)–P(2)	48.87	49.74
P(3)−C(13)−C(20)−P(4)	52.23	50.62
P(1)–P(3)–P(4)–P(2)	68.60	63.12
P(1)–Au(1)−Au(2)–P(2)	81.08	70.78
P(3)–Au(1)−Au(2)–P(4)	84.93	70.62
P(1)–Au(1)−Au(2)–P(4)	–98.51	–109.86
P(3)–Au(1)−Au(2)–P(2)	–95.48	–108.75

Table S2 Absorption and emission wavelengths (λ), oscillator strengths (f) and orbital compositions for singlet and triplet excited states of $[Au_2(dpephos)_2]^{2+}$ cation computed by TD DFT method.

Excited state	**λ**	**f**	(Assignment: H = HOMO, L = LUMO)
S_1	**291**	**0.0221**	**H → L (81%)**, H-1 → L+2 (9%), H → L+1 (4%)
S_2	286	0.0012	H-1 → L (47%), H → L+2 (35%), H-1 → L+1 (7%), H → L+1 (2%)
S_3	285	0.0005	H → L (11%), H → L+1 (73%), H-1 → L+2 (8%), H → L+2 (4%)
S_4	282	0.0064	H-1 → L (41%), H-1 → L+1 (39%), H → L+2 (16%)
S_5	275	0.0033	H-2 → L (84%), H-2 → L+1 (4%), H-1 → L+2 (3%)
S_6	274	0.0016	H-1 → L+1 (26%), H → L+2 (28%), H → L+3 (30%), H-2 → L (3%), H → L (3%)
T_1	**683**	**0**	**H → L (87%)**, H-24 → L (4%)

Table S3 Compositions of molecular orbitals involved in the main absorption and emission transitions of $[Au_2(dpephos)_2]^{2+}$ cation obtained from TD DFT analysis.

Transition	Orbital	Au atoms[a]			Phosphine ligands
		s	p	d	
$S_0 \rightarrow S_1$	HOMO	0	0.002	0.002	0.950
		0.001	0.038	0.007	
	LUMO	0	0.249	0.001	0.553
		0	0.197	0	
$T_1 \rightarrow S_0$	HOMO	0	0.002	0.003	0.792
		0	0.085	0.118	
	LUMO	0.017	0.238	0.016	0.362
		0.196	0.067	0.104	

[a] The first line and the second lines correspond to the Au1 and Au2 atoms respectively.

Thermochromic luminescence (298 vs. 77K)

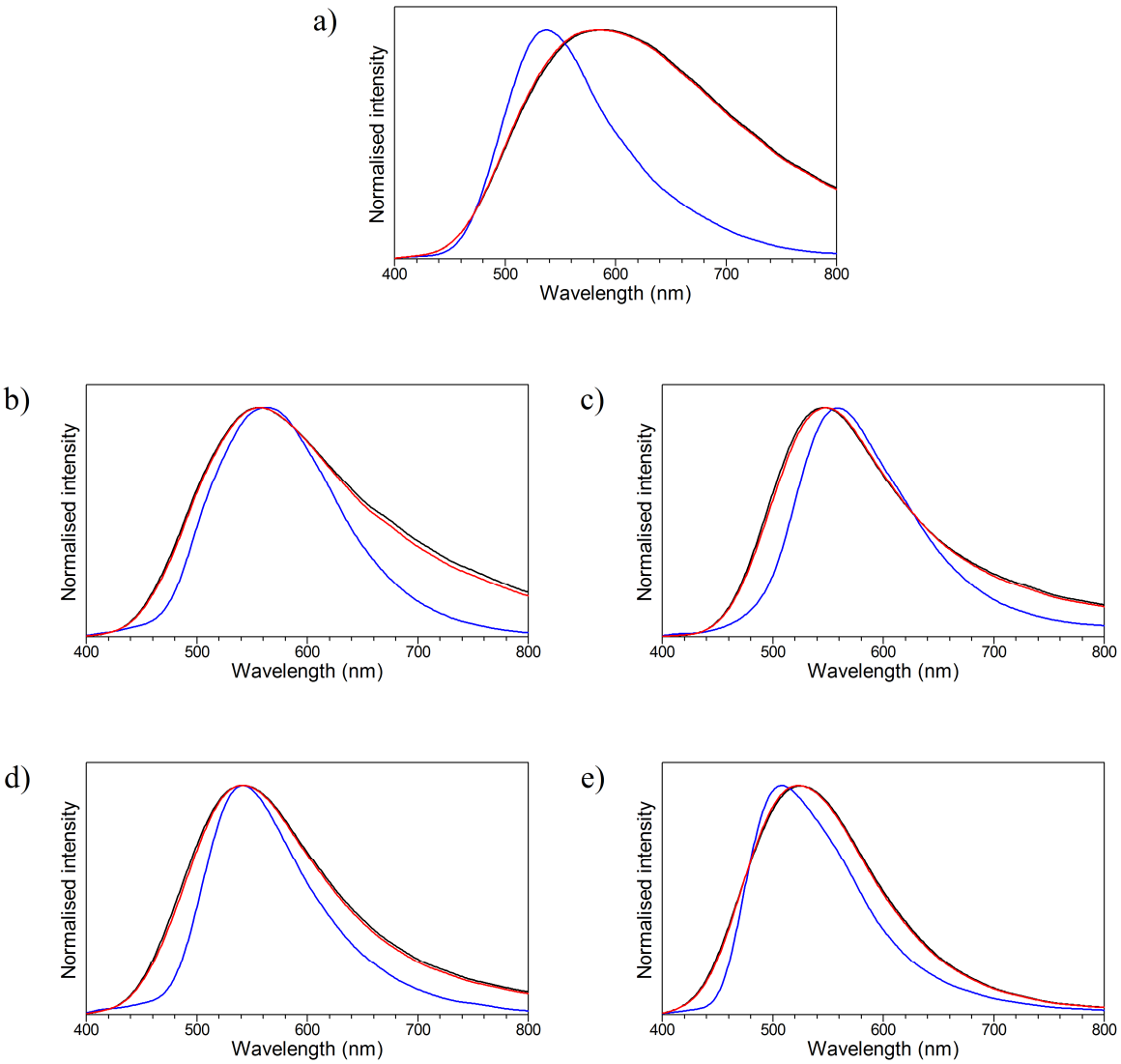

Fig. S22 Emission spectra of complexes **1** (a), **2** (b), **3** (c), **4** (d) and **5** (e) at 298 K (black and red lines), and 77 K (blue line) showing the reversible thermochromic luminescence upon excitation with 365 nm.

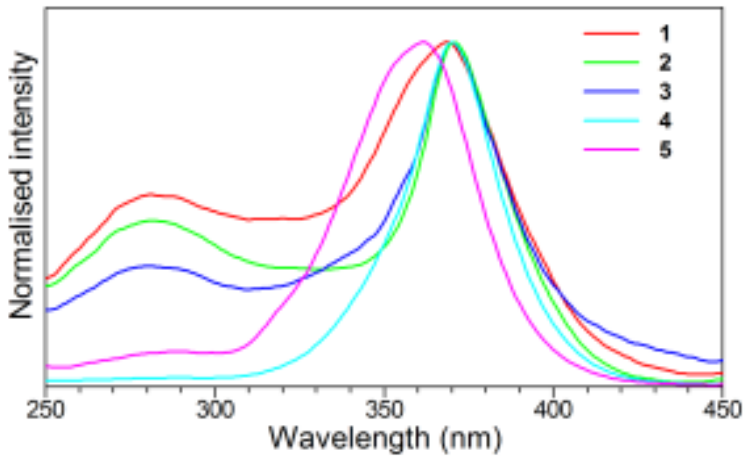

Fig. S23 Excitation spectra of crystals of **1**–**5** showing the HE band.

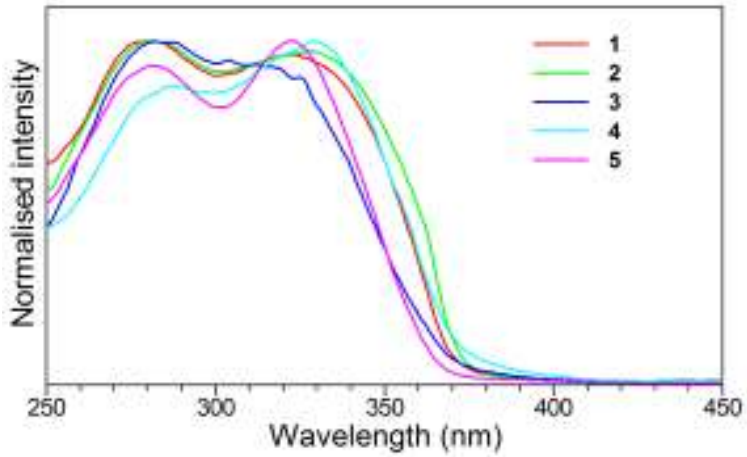

Fig. S24 Excitation spectra of crystals of **1**–**5** showing the LE band.

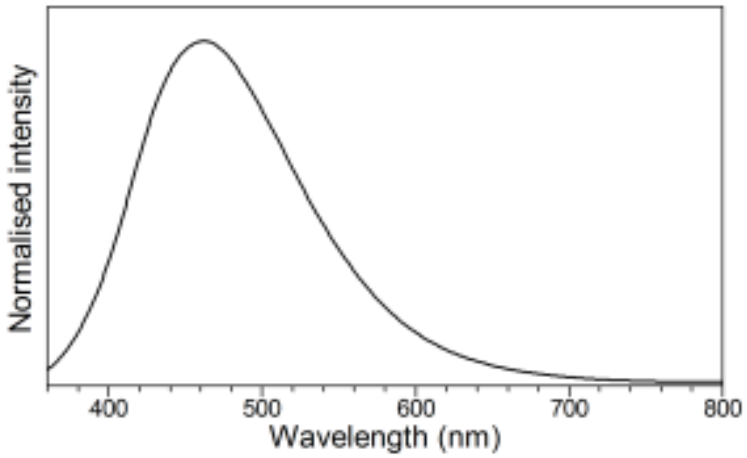

Fig. S25 Emission spectrum of dpephos ligand in glassy matrix (MeOH:EtOH, 4:1) at 77 K.

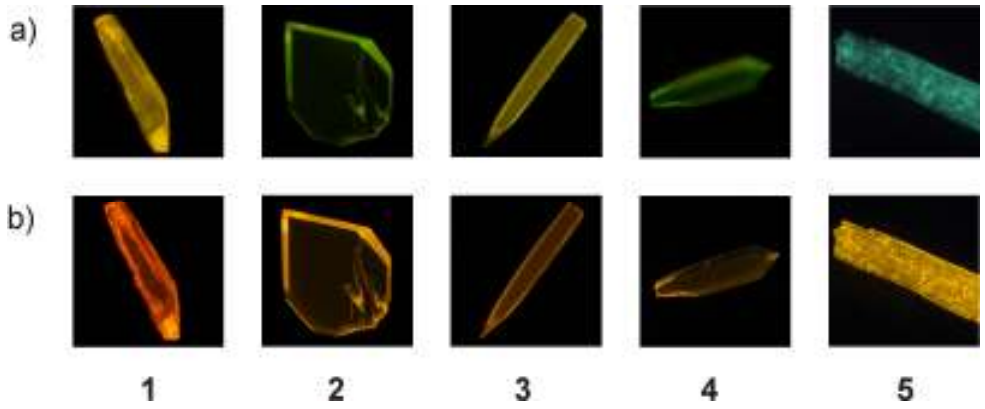

Fig. S26 Photographs of individual crystals of **1**–**5** taken under 365 nm (a) and 312 nm (b) UV lamp at room temperature.

Table S4 Emission maxima (in nm) and luminescent lifetimes (in μs) of HE and LE bands for individual crystals of **1**–**5** at 298 K.

Complex	λ_{ex} = 365 nm		λ_{ex} = 312 nm	
	λ_{max}	τ	λ_{max}	τ
1	590	1.8	631	19
2	566	2.7	640	20
3	550	2.5	672	22
4	537	1.4	588	20
5	530	1.5	570	19

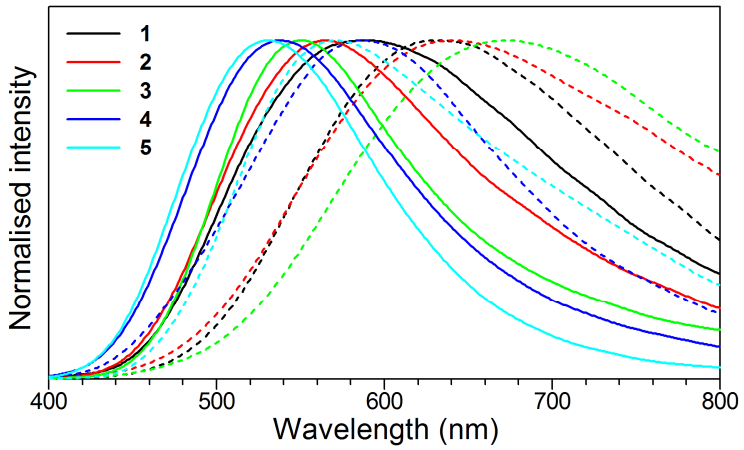

Fig. S27 Excitation wavelength-dependent emission spectra of individual crystals of **1**–**5** at 298 K (λ_{ex} = 365 nm, solid lines; λ_{ex} = 312 nm, dashed lines).

Mechanochromic luminescence

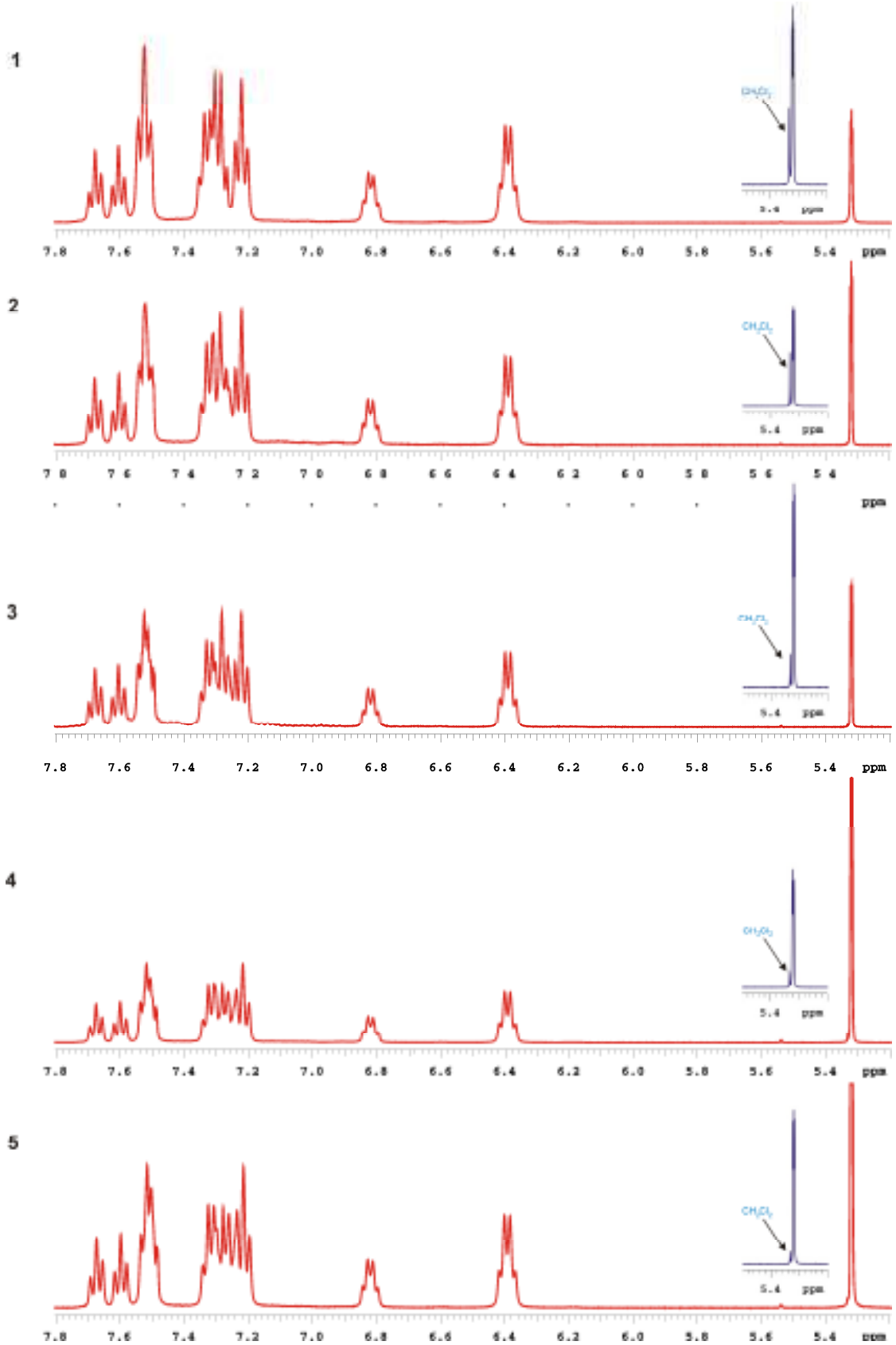

Fig. S28 ^{1}H-NMR spectra of ground **1**–**5** (red lines). Insets: details between 5.2 and 5.5 ppm from the ^{1}H-NMR spectra of unground crystals of **1**–**5** (blue lines).

Table S5 Emission data for crystalline-to-amorphous phase transition of complex **1**.

Complex	Stimuli	Cycle No.	λ_{ex} = 365 nm		λ_{ex} = 312 nm	
			λ_{max} (nm)	τ (μs)	λ_{max} (nm)	τ (μs)
1	-	-	592	1.7	611	21
	Grinding	1	688	18	670	18
1R	Fuming	1	640	17	637	19
single crystal of 1R			639	19	642	20

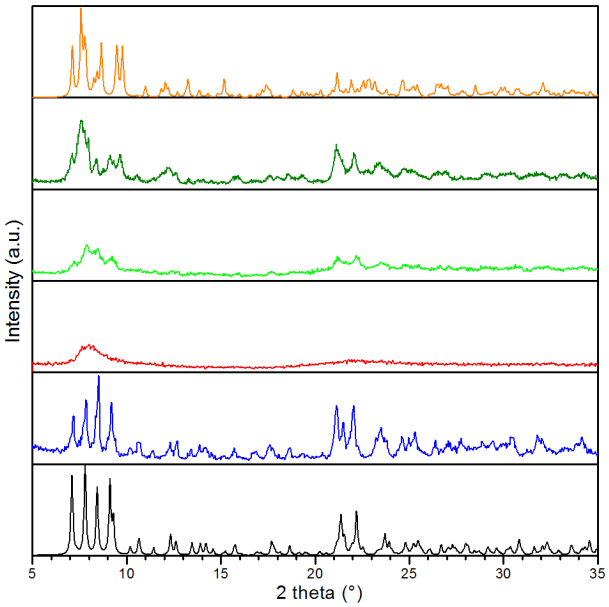

Fig. S29 PXRD diffractograms showing the simulated (black) and experimental patterns of unground **1** (blue), ground **1** (red), ground **1** after exposure to CH_2Cl_2 vapour (light green) and after addition of CH_2Cl_2, followed by solvent evaporation (dark green), as well as the simulated (orange) patterns of **1R**.

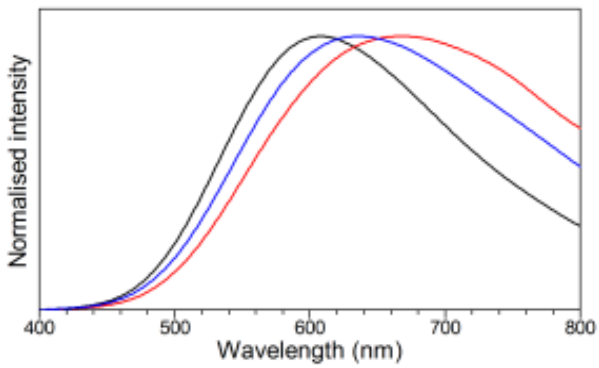

Fig. S30 Emission spectra showing the reversible mechanochromic luminescence of complex **1** (unground, black; ground, red and fumed, blue) upon excitation with 312 nm.

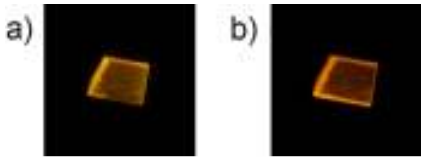

Fig. S31 Photographs of individual crystal of **1R** taken under 365 nm (a) and 312 nm (b) UV lamp at room temperature.

Table S6 Emission data for crystalline-to-amorphous phase transition of complex **2**.

Complex	Stimuli	Cycle No.	λ_{ex} = 365 nm		λ_{ex} = 312 nm	
			λ_{max} (nm)	τ (μs)	λ_{max} (nm)	τ (μs)
2	-	-	565	2.9	614	17
	Grinding	1	687	19	679	20
		2	683	18	678	19
		3	688	20	680	18
		4	684	20	681	21
	Fuming	1	570	3.6	614	16
		2	571	2.9	615	18
		3	569	3.2	616	17
		4	570	3.5	616	17

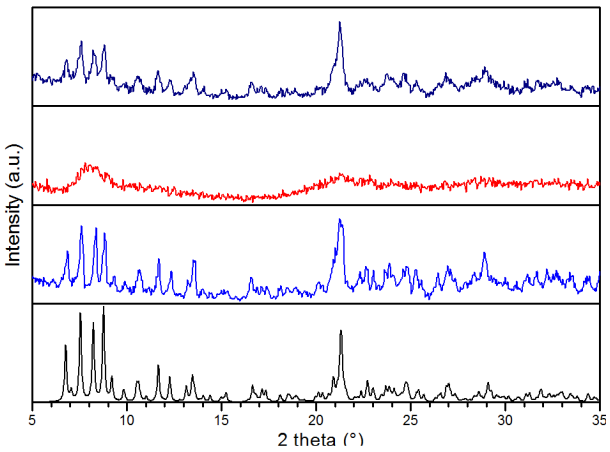

Fig. S32 PXRD diffractograms showing the simulated (black) and experimental patterns of unground (blue), ground (red) and CH_2Cl_2 fumed (dark blue) forms of **2**.

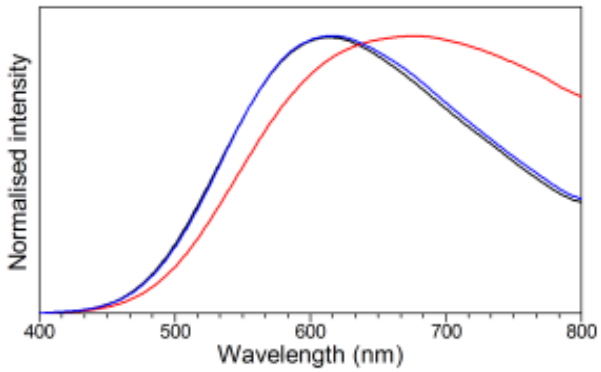

Fig. S33 Emission spectra showing the reversible mechanochromic luminescence of complex **2** (unground, black; ground, red and fumed, blue) upon excitation with 312 nm.

Table S7 Emission data for crystalline-to-amorphous phase transition of complex **3**.

Complex	Stimuli	Cycle No.	λ_{ex} = 365 nm		λ_{ex} = 312 nm	
			λ_{max} (nm)	τ (µs)	λ_{max} (nm)	τ (µs)
3	-	-	559	3.5	665	18
	Grinding	1	683	15	681	16
		2	681	16	679	16
		3	683	15	680	17
		4	684	17	680	15
	Fuming	1	561	4.1	665	17
		2	563	3.7	664	17
		3	563	3.9	666	18
		4	564	3.5	667	17

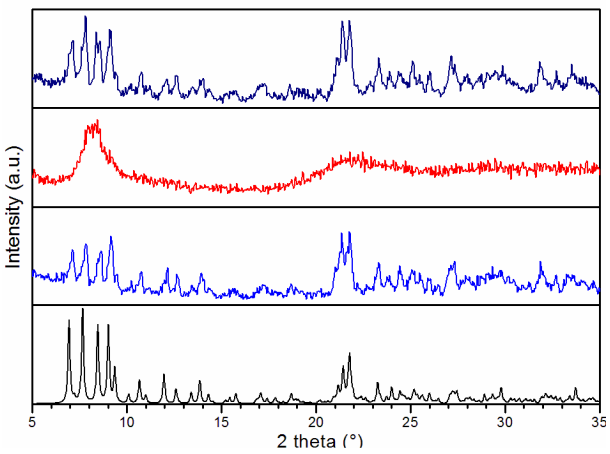

Fig. S34 PXRD diffractograms showing the simulated (black) and experimental patterns of unground (blue), ground (red) and CH_2Cl_2 fumed (dark blue) forms of **3**.

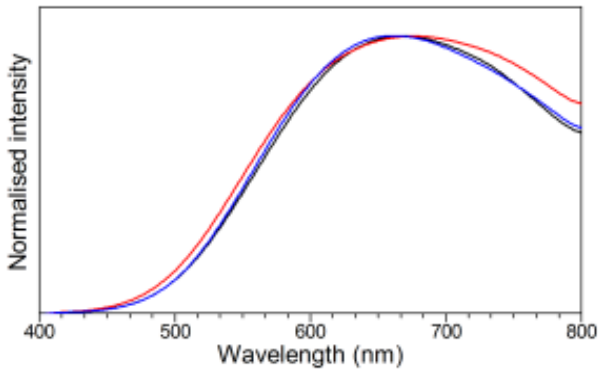

Fig. S35 Emission spectra showing the reversible mechanochromic luminescence of complex **3** (unground, black; ground, red and fumed, blue) upon excitation with 312 nm.

Table S8 Emission data for crystalline-to-amorphous phase transition of complex **4**.

Complex	Stimuli	Cycle No.	λ_{ex} = 365 nm		λ_{ex} = 312 nm	
			λ_{max} (nm)	τ (µs)	λ_{max} (nm)	τ (µs)
4	-	-	544	2.1	602	19
	Grinding	1	710	17	686	20
		2	715	17	688	20
		3	721	16	687	19
		4	718	18	686	20
	Fuming	1	546	2.7	604	18
		2	546	2.9	603	19
		3	548	3.0	603	19
		4	547	2.6	602	20

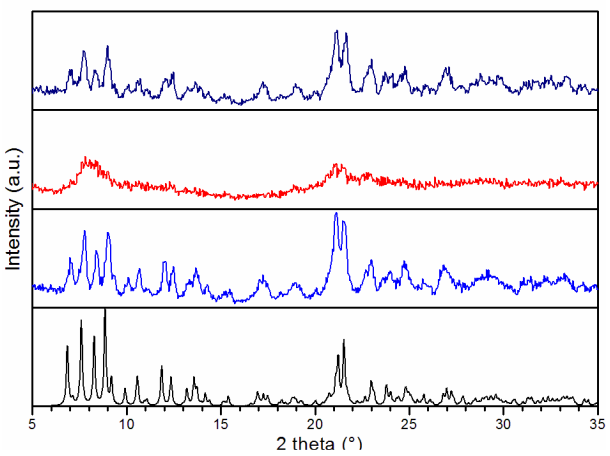

Fig. S36 PXRD diffractograms showing the simulated (black) and experimental patterns of unground (blue), ground (red) and CH_2Cl_2 fumed (dark blue) forms of **4**.

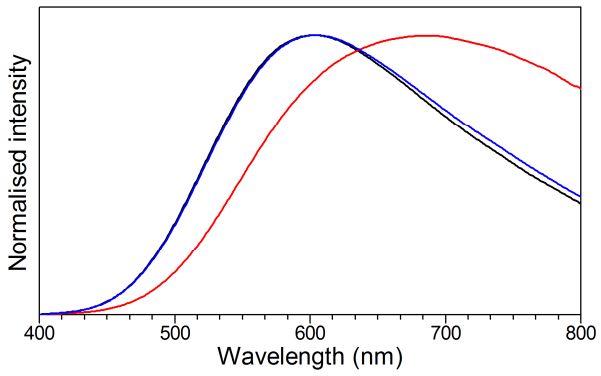

Fig. S37 Emission spectra showing the reversible mechanochromic luminescence of complex **4** (unground, black; ground, red and fumed, blue) upon excitation with 312 nm.

Table S9 Emission data for crystalline-to-amorphous phase transition of complex **5**.

Complex	Stimuli	Cycle No.	λ_{ex} = 365 nm		λ_{ex} = 312 nm	
			λ_{max} (nm)	τ (µs)	λ_{max} (nm)	τ (µs)
5	-	-	520	1.8	612	19
	Grinding	1	718	16	700	18
		2	715	18	701	18
		3	721	17	699	19
		4	715	16	699	17
	Fuming	1	519	2.9	612	18
		2	516	2.5	610	20
		3	517	2.8	611	19
		4	517	2.6	610	19

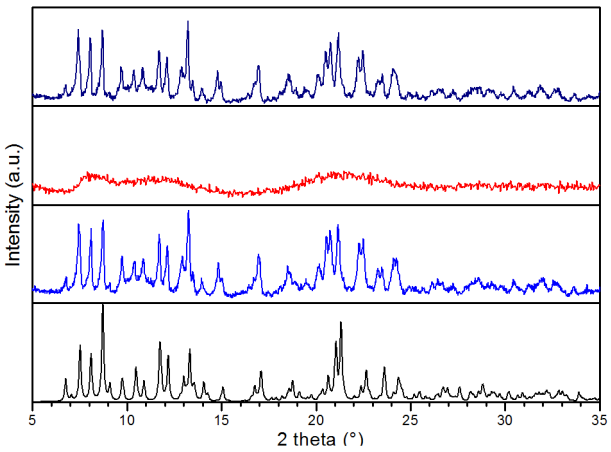

Fig. S38 PXRD diffractograms showing the simulated (black) and experimental patterns of unground (blue), ground (red) and CH_2Cl_2 fumed (dark blue) forms of **5**.

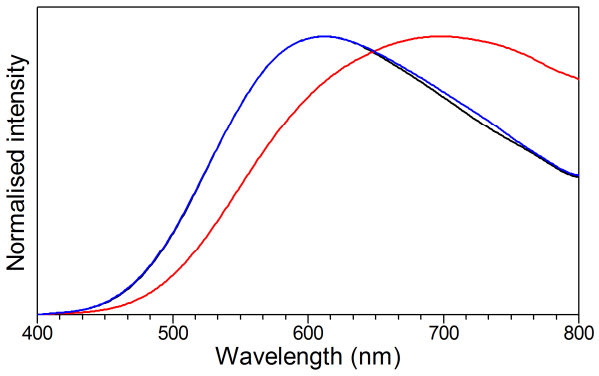

Fig. S39 Emission spectra showing the reversible mechanochromic luminescence of complex **5** (unground, black; ground, red and fumed, blue) upon excitation with 312 nm.

Table S10 Luminescence quantum yields of complexes **1**–**5** upon grinding and exposure to solvent vapours using 312 nm excitation at room temperature.

Complex	Ground	Fumed
1	0.06	0.11
2	0.05	0.12
3	0.07	0.10
4	0.06	0.10
5	0.05	0.11

Table S11 Relevant bond lengths (Å) and angles (°) of yellow (**1**) and reddish-orange (**1R)** luminescent forms.

	1	**1R**
Au(1)−P(1)	2.338(1)	2.327(2)
Au(1)−P(3)	2.333(1)	2.332(2)
Au(2)−P(2)	2.310(1)	2.320(2)
Au(2)−P(4)	2.309(1)	2.323(2)
Au(1)···Au(2)	3.609(2)	3.2383(5)
P(1)–Au(1)−P(3)	168.16(2)	160.7(1)
P(2)–Au(2)−P(4)	164.89(2)	169.6(1)
P(1)–C(1)–C(8)–P(2)	53.0(2)	49.4(1)
P(3)−C(13)−C(20)−P(4)	58.2(2)	51.5(2)
P(1)–P(3)–P(4)–P(2)	65.9(2)	69.3(2)
P(1)–Au(1)−Au(2)–P(2)	78.4(2)	80.8(2)
P(3)–Au(1)−Au(2)–P(4)	77.5(2)	83.8(2)
P(1)–Au(1)−Au(2)–P(4)	–101.3(2)	–100.2(2)
P(3)–Au(1)−Au(2)–P(2)	–102.9(2)	–95.1(2)

Details of the movie

The movie showing the reversibility of mechanochromic luminescence of **2** was recorded on a Nikon D5100 digital camera. The camera was in automatic white balance mode. In the early part of the movie, the crystals are shown under ambient light (white), then under 312 nm (orange), and 365 nm UV light (greenish-yellow). The crystals were ground by a spatula and pestle under UV irradiation with black light (365 nm). The change in the emission colour from yellowish-green to reddish-orange was observed, which intensified under 312 nm illumination. The 365 nm UV lamp was switched on, the ground sample was fumed with CH_2Cl_2 vapours, and the reddish-orange emission rapidly changed into greenish-yellow. Under 312 nm illumination the recovered solid shows reddish-orange emission. Then a second cycle with emission colour change from greenish-yellow to reddish-orange (under 365 nm) and orange to burning reddish-orange (under 312 nm) was recorded. It is worth noting that although the quantum yields of the ground complexes are practically excitation wavelength-independent, the absorbance of the ground **2** is much higher at 312 nm than at 365 nm. For this reason, the thin layer of the fine powdered sample on the wall of the mortar absorbs and emits much intensively upon 312 nm as compared to 365 nm.

Acknowledgements

The authors gratefully acknowledge the support by MTA (Hungarian Academy of Sciences) through the Lendület Programme (LP2012-21/2012).

We thank Ms. Laura Oláh's (Msc. student) for her contribution in the synthetic work. The authors are indebted to Dr. Attila Domján (NMR Spectroscopy Research Group, Institute of Organic Chemistry, Research Centre for Natural Sciences, Hungarian Academy of Sciences, Budapest, Hungary) for NMR spectroscopy measurements. We also thank Dr. Ágnes Gömöry and Dr. Olivér Ozohanics (MS Proteomics Research Group, Institute of Organic Chemistry, Research Centre for Natural Sciences, Hungarian Academy of Sciences, Budapest, Hungary) for HRMS-ESI measurements.

References

[1] *Gaussian 09*, Revision C.01, M. J. Frisch, G. W. Trucks, H. B. Schlegel, G. E. Scuseria, M. A. Robb, J. R. Cheeseman, G. Scalmani, V. Barone, B. Mennucci, G. A. Petersson, H. Nakatsuji, M. Caricato, X. Li, H. P. Hratchian, A. F. Izmaylov, J. Bloino, G. Zheng, J. L. Sonnenberg, M. Hada, M. Ehara, K. Toyota, R. Fukuda, J. Hasegawa, M. Ishida, T. Nakajima, Y. Honda, O. Kitao, H. Nakai, T. Vreven, J. A. Montgomery, Jr., J. E. Peralta, F. Ogliaro, M. Bearpark, J. J. Heyd, E. Brothers, K. N. Kudin, V. N. Staroverov, R. Kobayashi, J. Normand, K. Raghavachari, A. Rendell, J. C. Burant, S. S. Iyengar, J. Tomasi, M. Cossi, N. Rega, J. M. Millam, M. Klene, J. E. Knox, J. B. Cross, V. Bakken, C. Adamo, J. Jaramillo, R. Gomperts, R. E. Stratmann, O. Yazyev, A. J. Austin, R. Cammi, C. Pomelli, J. W. Ochterski, R. L. Martin, K. Morokuma, V. G. Zakrzewski, G. A. Voth, P. Salvador, J. J. Dannenberg, S. Dapprich, A. D. Daniels, Ö. Farkas, J. B. Foresman, J. V. Ortiz, J. Cioslowski, and D. J. Fox, *Gaussian*, Inc., Wallingford CT, **2009**.

[2] Y. Zhao and D. G. Truhlar, *Acc. Chem. Res.*, **2008**, *41*, 157–167.

[3] Ugo Varetto, Molekel 5.4, http:// http://ugovaretto.github.io/molekel/